Astronomy
&
Astrophysics

Metallicity estimates for old star clusters in M 33

Jun Ma, Xu Zhou, and Jiansheng Chen

National Astronomical Observatories, Chinese Academy of Sciences, Beijing 100012, PR China

Abstract. Using the theoretical stellar population synthesis models of BC96, Kong et al. (2003) showed that some BATC colors and color indices could be used to disentangle the age and metallicity effect. They found that there is a very good relation between the flux ratio of L_{8510}/L_{9170} and the metallicity for stellar populations older than 1 Gyr. In this paper, based on the Kong et al. results and on the multicolor spectrophotometry of Ma et al. (2001, 2002a,b,c), we estimate the metallicities of 31 old star clusters in the nearby spiral galaxy M 33, 23 of which are "true" globular clusters. The results show that most of these old clusters are metal poor. We also find that the ages and metal abundance for these old star clusters of M 33 do not vary with deprojected radial position.

Key words. galaxies: individual: M 33 – galaxies: evolution – galaxies: star clusters

1. Introduction

Globular clusters (GCs) are thought to be among the oldest radiant objects in the Universe. They are simple coeval stellar systems which formed on a very short timescale during phases of intense star formation in host galaxies. The GCs of the Milky Way probe the manner in which our Galaxy formed. Studies of similar populations in other galaxies can reveal the properties of these galaxies soon after their formation. For example, the widely varying specific frequency of GCs in individual galaxies indicates that cluster formation is almost certainly affected by the local environment with the host galaxy.

M 33, at a distance of 850 kpc, is the third-brightest member of the Local Group, and is classified as a late-type ScII-III spiral (1999). This galaxy represents a morphological type intermediate between the largest "early-type" spirals and the dwarf irregulars in the Local Group (Chandar et al. 1999a). M 33 subtends 1° on the sky. Its large angular extent and favorable inclination $i = 56°$ (Regan & Vogel 1994) make it suitable for studies of stellar content. However, its large size makes its study difficult. The Beijing-Arizona-Taiwan-Connecticut (BATC) Multicolor Sky Survey (Fan et al. 1997; Zheng et al. 1999) obseves M 33 as part of its galaxy calibration program.

Before Chandar et al. (1999a,b,c, 2001, 2002), the system of clusters in M 33 were not well studied, although detection, and photometry and spectrophotometry have been obtained (see details from Hiltner 1960; Kron & Mayall 1960; Melnick & D'Odorico 1978; Christian & Schommer 1982, 1988; Huchra et al. 1996). Now, a database of about 400 star clusters is available from the ground-based work, and from the *Hubble Space Telescope* (HST) images.

Using the theoretical stellar population synthesis models of Bruzual & Charlot (1996, unpublished, hereafter BC96) and multicolor photometry, Kong et al. (2000) studied the age, metallicity, and interstellar-medium reddening distribution for M 81. When they convolved the spectral energy distributions (SEDs) of BC96 with the BATC filter profiles to obtain the optical and near-integrated luminosity, they found that, among all the BATC filter bands, the color index centered at 8510 Å is much more sensitive to the metallicity than to the age. The center of this filter band is near the Ca II triplets ($\lambda\lambda = 8498, 8542, 8662$ Å) (hereafter CaT). As Zhou (1991) noted, that the strength of the CaT depends on the effective temperature, surface gravity, and the metallicity in late-type stars. A very good relation between the flux ratio of $I_{8510} \equiv L_{8510}/L_{9170}$ and the metallicity was found for stellar populations older than 1 Gyr in Kong et al. (2000).

In this paper, we estimate the metallicities of the 31 old star clusters that were detected by Christian & Schommer (1982), Chandar et al. (1999a, 2001), and by Mochejska et al. (1998) in M 33 using the relation of Kong et al. (2000). The ages of all these sample star clusters were estimated by Ma et al. (2001, 2002a,b,c) by comparing the BC96 simple stellar population synthesis models with the integrated photometric measurements.

The outline of the paper is as follows. Sample selection, observations and data reduction are given in Sect. 2. Section 3 presents the spectral synthesis models. In Sect. 4, we provide a brief description of the method of Kong et al. (2000), and estimate the metallicities of 31 sample old star clusters. Some statistical properties of old star clusters are investigated in Sect. 5. In Sect. 6, we give our major results and some discussions.

Send offprint requests to: Jun Ma,
e-mail: `majun@vega.bac.pku.edu.cn`

2. Sample of star clusters, observations and data reduction

2.1. Sample of old star clusters

The sample of star clusters in this paper is from Ma et al. (2001, 2002a,b,c), who presented multicolor photometry and estimated the ages using BC96 models for 180 star clusters in M 33. The RA and Dec of these clusters are from Christian & Schommer (1982), Chandar et al. (1999a, 2001), or Mochejska et al. (1998). Christian & Schommer (1982) detected more than 250 nonstellar objects using 14×14 inch^2 unfiltered, un-baked, IIa-O focus plates exposed for 150 minutes with the Kitt Peak 4 m Richey-Chrétien (R-C) direct camera. Chandar et al. (1999a, 2001) used 55 multiband HST WFPC2 fields to search for star clusters much closer to the nucleus of M 33 than previous studies, and detected 162 star clusters, 131 of which were previously unknown. Mochejska et al. (1998) detected 51 globular cluster candidates in M 33, 32 of which were not previously cataloged, using the data collected in the DIRECT project (1998; 1998). Ma et al. (2001, 2002a,b,c) obtained the SEDs of the 180 clusters by aperture photometry, and estimated their ages using the theoretical evolutionary population synthesis methods. In Ma et al. (2001), there are 10 clusters, the ages of which are older than 1 Gyr. We exclude three star clusters of these 10 because of their low signal-to-noise ratios. Also, cluster 54 in Chandar et al. (1999a) is U137 in Christian & Schommer (1982). In Ma et al. (2002b), there are 22 clusters older than 1 Gyr. However, the ratios of signal-to-noise of 11 clusters are not high enough, and are not included in this sample. In Ma et al. (2002c), there are 5 clusters older than 1 Gyr. The signal-to-noise ratio of cluster 2 is not high enough, and is also not included in this sample. Altogether, there are 31 old star clusters in this paper. Figure 1 is the image of M 33 in filter BATC07 (5785 Å), the circles indicate the positions of the sample clusters. By comparing the photometric measurements to integrated colors from theoretical models by Bertelli et al. (1994), Chandar et al. (1999b, 2002) estimated ages for 23 old star clusters in common. Table 1 lists the comparison of age estimates with previously results (Chandar et al. 1999b, 2002). Except for clusters 49 and 59 of Chandar et al. (1999a), the ages estimated by Ma et al. (2001, 2002a,b,c) are consistent with the ones estimated by Chandar et al. (1999b, 2002). Cluster 49, the $B - V$ value of which is very large 0.824 (Chandar et al. 1999b), should be an old cluster. Our sample includes 23 "true" globular clusters, which have $(B - V)_0 \geq 0.6$ or $(V - I)_0 \geq 0.78$, colors typical of Galactic GCs (Chandar et al. 2001).

2.2. Observations and data reduction

The large field multicolor observations of the spiral galaxy M 33 were collected using the Ford Aerospace 2048×2048 CCD mosaic camera on the 60/90 cm f/3 Schmidt telescope of the Xinglong station of the National Astronomical Observatories. The field of view of the CCD is $58' \times 58'$ with a pixel scale of $1''.7$. The typical seeing of the Xinglong station is $2''$. The multicolor BATC filter system, which was specifically designed to avoid contamination from the
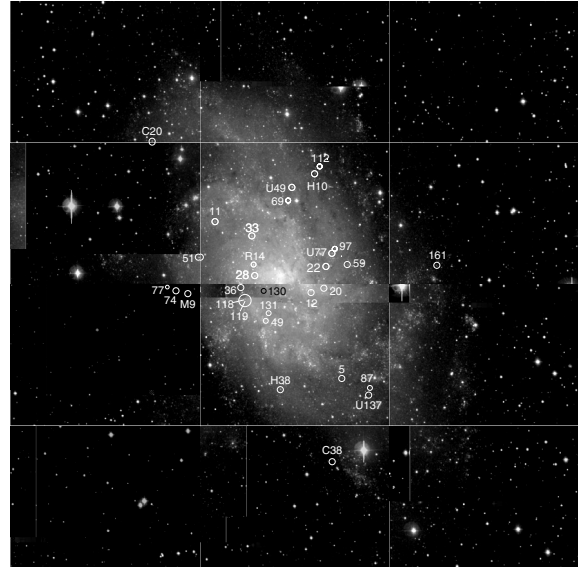

Fig. 1. The image of M 33 in filter BATC07 (5785 Å) and the positions of the sample star clusters. The center of the image is located at RA = $01^h33^m50^s.58$ Dec = $30°39'08''.4$ (J2000.0). North is up and east is to the left.

brightest and most variable night sky emission lines, includes 15 intermediate-band filters, covering the total optical wavelength range from 3000 to 10 000 Å. It is defined the magnitude zero points similar to the spectrophotometric AB magnitude system, a $\tilde{f}_\nu$ monochromatic system (Oke & Gunn 1983) based on the SEDs of the four F sub-dwarfs, HD 19445, HD 84937, BD +26°2606, and BD +17°4708. The advantage of the AB magnitude system is that the magnitude is directly related to physical units. The BATC magnitude system is defined as the AB magnitude system,

$$m_{\text{batc}} = -2.5 \log \tilde{F}_\nu - 48.60, \tag{1}$$

where $\tilde{F}_\nu$ is the appropriately averaged monochromatic flux in units of erg s^{-1} cm^{-2} Hz^{-1} at the effective wavelength of the specific passband. In the BATC system (Yan et al. 2000), $\tilde{F}_\nu$ is defined as

$$\tilde{F}_\nu = \frac{\int d(\log \nu) f_\nu R_\nu}{\int d(\log \nu) R_\nu}, \tag{2}$$

which links the magnitude to the number of photons detected by the CCD rather than to the input flux (Fukugita et al. 1996). In this equation, R_ν is the system response, f_ν is the SED of the source.

The images of M 33 covering the whole optical body of M 33 were accumulated in 13 intermediate band filters with a total exposure time of about 37.25 hours from September 23, 1995 to August 28, 2000. Data reduction, by bias subtraction and flat-fielding with dome flats, was performed with the automatic data reduction software PIPELINE I developed for the BATC multicolor sky survey (1996; 1999). The dome flat-field images were taken by using a diffuse plate in front of the correcting plate of the Schmidt telescope. We performed photometric calibration of the M 33 images using the Oke-Gunn primary flux standard stars HD 19445, HD 84937, BD +26°2606,

Table 1. Comparion of age estimates with previous measurements.

Cluster[a]	Chandar et al. log age (yr)	Ma et al. log age (yr)
U 49	9.2 ± 0.1	9.60
R 12	9.7 ± 0.1	10.00
R 14	10.2 ± 0.2	9.11
M 9	9.2 ± 0.1	9.63
U 77	9.15 ± 0.15	9.20
H 38	9.25 ± 0.15	9.70
C 20	9.2 ± 0.1	9.95
C38	8.9 ± 0.1	9.28
H 10	9.25 ± 0.15	9.90
U 137	9.35 ± 0.15	10.27
CBF 11	9.50 ± 0.30	10.30
CBF 20	10.1 ± 0.20	9.54
CBF 22	9.25 ± 0.15	9.26
CBF 28	10.2 ± 0.40	9.80
CBF 49	7.90 ± 0.20	9.34
CBF 59	7.40 ± 0.20	9.11
CBF 69	9.2 ± 0.1	9.76
CBF 74	9.3 ± 0.1	9.32
CBF 97	9.3 ± 0.2	10.28
CBF 112	8.8 ± 0.2	9.21
CBF 118	9.15 ± 0.15	9.16
CBF 161	9.1 ± 0.1	9.23
M 12	9.4 ± 0.2	9.63

[a] CBF identifications are from Chandar et al. (1999a, 2001); M identifications are from Mochejska et al. (1998); The others are from Christian & Schommer (1982).

Table 2. Parameters of the BATC filters and statistics of observations.

No.	Name	cw[a](Å)	Exp. (hr)	N.img[b]	rms[c]
1	BATC03	4210	00:55	04	0.024
2	BATC04	4546	01:05	04	0.023
3	BATC05	4872	03:55	19	0.017
4	BATC06	5250	03:19	15	0.006
5	BATC07	5785	04:38	17	0.011
6	BATC08	6075	01:26	08	0.016
7	BATC09	6710	01:09	08	0.006
8	BATC10	7010	01:41	08	0.005
9	BATC11	7530	02:07	10	0.017
10	BATC12	8000	03:00	11	0.003
11	BATC13	8510	03:15	11	0.005
12	BATC14	9170	04:45	25	0.011
13	BATC15	9720	05:00	26	0.009

[a] Central wavelength for each BATC filter.
[b] Image numbers for each BATC filter.
[c] Zero point error, in magnitude, for each filter as obtained from the standard stars.

and BD +17°4708, which were observed during photometric nights (see details from Yan et al. 2000; Zhou et al. 2001).

Using the images of the standard stars observed on photometric nights, we derive iteratively the extinction curves and the slight variation of the extinction coefficients with time (Zhou et al. 2001). The extinction coefficients at any given time in a night $[K + \Delta K(UT)]$ and the zero point of the instrumental magnitude (C) were obtained by

$$m_{\text{batc}} = m_{\text{inst}} + [K + \Delta K(UT)]X + C, \tag{3}$$

where X is air mass. The instrumental magnitudes (m_{inst}) of the selected bright, isolated and unsaturated stars on the M 33 images of the same photometric nights can be readily transformed to the BATC AB magnitude system (m_{batc}). We calibrated the photometry on the combined images by comparing the magnitudes of these stars to determine a mean magnitude offset to the photometric images. Table 2 lists the parameters of the BATC filters and the statistics of observations. Column 6 of Table 2 gives the zero point error, in magnitude, for the standard stars in each filter. The formal errors we obtain for these stars in the 13 BATC filters are ≲0.02 mag. This indicates that we can define the standard BATC system to an accuracy of ≲0.02 mag.

2.3. Integrated photometry

For each star cluster, aperture photometry was used to obtain magnitudes. To avoid contamination from nearby objects, we adopt a small aperture of 6″.

Table 3. SEDs of 31 old star clusters.

Cluster[a]	03	04	05	06	07	08	09	10	11	12	13	14	15
(1)	(2)	(3)	(4)	(5)	(6)	(7)	(8)	(9)	(10)	(11)	(12)	(13)	(14)
U 49	16.99	16.56	16.46	16.27	16.06	15.98	15.82	15.78	15.70	15.58	15.52	15.48	15.40
	0.022	0.018	0.014	0.015	0.010	0.011	0.011	0.010	0.010	0.009	0.010	0.012	0.012
R 12	17.34	16.81	16.62	16.43	16.15	16.11	15.90	15.83	15.77	15.68	15.56	15.51	15.44
	0.049	0.036	0.027	0.029	0.020	0.021	0.022	0.023	0.022	0.019	0.021	0.020	0.024
R 14	17.55	17.04	16.84	16.59	16.21	16.14	15.91	15.81	15.66	15.55	15.43	15.32	15.20
	0.052	0.037	0.027	0.028	0.019	0.021	0.017	0.018	0.020	0.016	0.017	0.017	0.021
M 9	17.82	17.48	17.38	17.17	16.96	16.90	16.73	16.68	16.60	16.53	16.45	16.39	16.38
	0.046	0.034	0.025	0.026	0.016	0.018	0.016	0.018	0.018	0.017	0.025	0.021	0.026
U 77	17.94	17.51	17.38	17.20	17.05	16.97	16.77	16.75	16.68	16.59	16.58	16.49	16.41
	0.066	0.047	0.042	0.039	0.025	0.024	0.033	0.024	0.030	0.028	0.030	0.031	0.044
H 38	18.03	17.68	17.52	17.27	17.06	16.99	16.80	16.71	16.69	16.61	16.55	16.46	16.49
	0.035	0.028	0.021	0.020	0.016	0.016	0.015	0.015	0.016	0.015	0.022	0.019	0.026
C 20	18.44	18.05	17.87	17.70	17.50	17.42	17.24	17.26	17.13	17.00	16.90	16.84	16.81
	0.037	0.026	0.022	0.022	0.017	0.020	0.017	0.020	0.019	0.019	0.025	0.021	0.039
C 38	18.71	18.35	18.28	18.05	17.98	17.88	17.78	17.70	17.73	17.73	17.80	17.80	17.72
	0.080	0.050	0.040	0.058	0.029	0.040	0.032	0.037	0.034	0.041	0.058	0.061	0.089
H 10	19.27	18.73	18.54	18.21	17.96	17.76	17.53	17.51	17.31	17.21	17.19	17.10	17.03
	0.093	0.055	0.043	0.038	0.030	0.030	0.033	0.031	0.029	0.029	0.033	0.036	0.053
U 137	19.21	18.88	18.68	18.42	18.22	18.10	17.88	17.80	17.81	17.74	17.71	17.54	17.61
	0.082	0.058	0.043	0.043	0.030	0.030	0.029	0.031	0.033	0.036	0.049	0.042	0.065
CBF 11	19.56	19.05	18.99	18.82	18.50	18.52	18.19	18.11	17.99	17.95	17.67	17.62	17.54
	0.153	0.098	0.080	0.085	0.063	0.075	0.052	0.053	0.050	0.067	0.081	0.046	0.071
CBF 20	19.11	18.76	18.70	18.45	18.31	18.25	18.05	17.83	17.70	17.71	17.52	17.39	17.30
	0.102	0.077	0.063	0.063	0.054	0.061	0.048	0.043	0.040	0.055	0.072	0.038	0.058
CBF 22	18.66	18.23	18.13	18.01	17.76	17.79	17.74	17.63	17.60	17.49	17.56	17.49	17.32
	0.065	0.046	0.037	0.040	0.032	0.038	0.035	0.034	0.035	0.043	0.071	0.040	0.056
CBF 28	17.26	16.75	16.60	16.46	16.16	16.15	15.97	15.91	15.87	15.78	15.72	15.69	15.66
	0.024	0.017	0.013	0.014	0.010	0.012	0.010	0.010	0.010	0.011	0.015	0.010	0.014
CBF 49	19.37	18.54	18.56	18.52	18.08	18.07	17.86	17.91	17.93	17.74	17.80	17.81	17.75
	0.151	0.073	0.065	0.078	0.049	0.057	0.046	0.050	0.054	0.059	0.094	0.059	0.090
CBF 59	18.47	18.29	18.28	18.19	17.92	17.98	17.87	17.69	17.48	17.38	17.34	17.16	17.05
	0.046	0.038	0.034	0.037	0.033	0.036	0.031	0.029	0.026	0.034	0.050	0.028	0.041
CBF 69	19.36	19.10	18.99	18.53	18.62	18.48	18.34	18.28	18.19	18.21	17.96	17.90	18.08
	0.154	0.125	0.135	0.155	0.100	0.088	0.093	0.087	0.099	0.103	0.106	0.102	0.163
CBF 74	19.93	19.43	19.14	18.87	18.68	18.59	18.47	18.40	18.41	18.16	18.28	18.09	18.08
	0.201	0.142	0.095	0.100	0.064	0.069	0.064	0.068	0.072	0.061	0.098	0.076	0.101
CBF 77	18.53	18.33	18.35	18.04	18.08	17.80	17.82	17.82	17.64	17.50	17.57	17.46	17.09
	0.061	0.045	0.039	0.046	0.032	0.036	0.030	0.036	0.035	0.028	0.049	0.037	0.054
CBF 87	19.91	19.44	19.22	18.96	18.89	18.68	18.53	18.45	18.50	18.35	18.19	18.23	18.28
	0.143	0.090	0.060	0.057	0.045	0.051	0.051	0.052	0.055	0.047	0.072	0.075	0.102

optical and near-infrared integrated luminosity. The integrated luminosity $L_{\lambda_i}(t, Z)$ of the ith BATC filter can be calculated as

$$L_{\lambda_i}(t, Z) = \frac{\int F_\lambda(t, Z)\varphi_i(\lambda)\mathrm{d}\lambda}{\int \varphi_i(\lambda)\mathrm{d}\lambda}, \qquad (4)$$

where $F_\lambda(t, Z)$ is the SED of the BC96 of metallicity Z at age t, $\varphi_i(\lambda)$ is the response functions of the ith filter of the BATC filter system ($i = 3, 4, \ldots, 15$), respectively. To avoid using distance-dependent parameters, we calculate the integrated colors of a BC96 relative to the BATC filter BATC08 ($\lambda = 6075$ Å):

$$C_{\lambda_i}(t, Z) = L_{\lambda_i}(t, Z)/L_{6075}(t, Z). \qquad (5)$$

As a result, we obtain intermediate-band colors for 6 metallicities from $Z = 0.0004$ to $Z = 0.1$. Then, we determined the ages

and best-fit models of metallicity by minimizing the difference between the intrinsic and integrated colors of BC96,

$$R^2(n, t, Z) = \sum_{i=3}^{15} \left[C_{\lambda_i}^{\mathrm{intr}}(n) - C_{\lambda_i}^{\mathrm{ssp}}(t, Z) \right]^2, \qquad (6)$$

where $C_{\lambda_i}^{\mathrm{ssp}}(t, Z)$ represents the integrated color in the ith filter of a SSP with age t and metallicity Z, and $C_{\lambda_i}^{\mathrm{intr}}(n)$ is the intrinsic integrated color for nth starcluster. For convenience, we also list the ages of sample star clusters of this paper in Col. 5 of Table 4. The uncertainties in the age estimates arising from photometric uncertainties are 0.2 or so, i.e., age $\pm$ 0.2 × age [log yr], and are formal errors that do not include the model uncertainties. The star cluster ages obtained in this paper are model-dependent and do not represent "absolute values". Uncertainties exist in the stellar evolution, in

Table 3. continued.

Cluster[a]	03	04	05	06	07	08	09	10	11	12	13	14	15
(1)	(2)	(3)	(4)	(5)	(6)	(7)	(8)	(9)	(10)	(11)	(12)	(13)	(14)
CBF 87	19.91	19.44	19.22	18.96	18.89	18.68	18.53	18.45	18.50	18.35	18.19	18.23	18.28
	0.143	0.090	0.060	0.057	0.045	0.051	0.051	0.052	0.055	0.047	0.072	0.075	0.102
CBF 97	19.18	18.81	18.64	18.49	18.29	18.17	17.83	17.79	17.72	17.61	17.53	17.37	17.44
	0.125	0.105	0.091	0.086	0.067	0.068	0.063	0.059	0.069	0.057	0.065	0.056	0.094
CBF 112	19.08	18.79	18.74	18.51	18.49	18.40	18.33	18.33	18.22	18.04	18.08	18.07	18.17
	0.082	0.071	0.059	0.063	0.053	0.056	0.059	0.065	0.071	0.063	0.080	0.082	0.161
CBF 118	18.32	18.00	17.88	17.66	17.52	17.39	17.27	17.13	17.05	17.10	16.97	16.72	16.78
	0.163	0.154	0.123	0.126	0.091	0.094	0.087	0.084	0.084	0.084	0.089	0.066	0.089
CBF 119	18.48	18.16	18.09	17.87	17.72	17.60	17.54	17.34	17.26	17.31	17.16	16.90	16.95
	0.160	0.154	0.122	0.126	0.093	0.094	0.096	0.082	0.086	0.081	0.086	0.063	0.089
CBF 130	17.67	17.32	17.48	17.22	17.43	17.06	16.85	16.81	16.78	17.13	16.66	16.68	16.60
	0.089	0.078	0.079	0.089	0.087	0.080	0.066	0.075	0.086	0.114	0.087	0.093	0.108
CBF 131	18.27	17.87	17.87	17.75	17.54	17.48	17.32	17.32	17.32	17.34	17.21	17.24	17.08
	0.113	0.089	0.074	0.079	0.052	0.054	0.049	0.052	0.061	0.058	0.069	0.077	0.085
CBF 161	19.364	19.028	18.869	18.660	18.457	18.339	18.180	18.074	17.956	17.942	17.951	17.631	17.631
	0.077	0.054	0.039	0.034	0.033	0.033	0.034	0.036	0.035	0.038	0.059	0.043	0.078
M 5	19.17	18.70	18.52	18.28	18.05	17.94	17.78	17.63	17.63	17.53	17.61	17.38	17.42
	0.084	0.051	0.037	0.043	0.031	0.034	0.032	0.036	0.037	0.035	0.050	0.038	0.076
M 12	17.99	17.67	17.53	17.29	17.15	17.04	16.83	16.78	16.74	16.64	16.53	16.41	16.36
	0.116	0.114	0.089	0.086	0.064	0.064	0.038	0.051	0.055	0.051	0.056	0.058	0.061
M 33	17.06	16.65	16.52	16.35	16.16	16.11	15.97	15.93	15.87	15.74	15.69	15.64	15.53
	0.045	0.034	0.026	0.031	0.022	0.024	0.022	0.022	0.023	0.020	0.022	0.021	0.024
M 51	18.07	17.70	17.64	17.52	17.35	17.32	17.21	17.18	17.12	17.06	17.01	16.98	16.85
	0.030	0.022	0.018	0.021	0.017	0.019	0.019	0.022	0.023	0.024	0.038	0.035	0.042

[a] CBF identifications are from Chandar et al. (1999a, 2001); M identifications are from Mochejska et al. (1998); The others are from Christian & Schommer (1982).

the physics of the stellar structure and in the spectral libraries. For example, Charlot et al. (1996) evaluated the uncertainties in stellar population synthesis models by analyzing in detail the origin of the discrepancies between three models (Bertelli et al. 1994; Worthey 1994, BC96), and showed the main uncertainties originate from the underlying stellar evolution theory, the color-temperature scale of giant stars, and the flux libraries. Cardiel et al. (2003) also discussed in detail the problem of disentangling stellar population properties using the spectroscopic data. Vazdekis et al. (2001) investigated the origin of the discrepancy between the spectroscopic age and the CMD age for the Milky Way GC 47 Tuc, and found that the α-enhanced isochrones with atomic diffusion included can provide a good fit to the CMD of 47 Tuc and lead to a spectroscopic age in better agreement with the CMD age.

4. Metallicity estimates

4.1. Correlation between color index and metallicity

To study the integrated properties of the stellar population in M 81, Kong et al. (2000) used the simple stellar population synthesis models of BC96. First, they convolved the SEDs of BC96 with the BATC filter profiles to obtain the optical and near-infrared integrated luminosity. When they plot the relations between color and age, they found that, among all the BATC filter bands, the color index centered at 8510 Å is much more sensitive to the metallicity than to the age (see Fig. 3 of Kong et al. 2000 for details). The center of this filter

band (8510 Å) is near the CaT. A good relationship between the flux ratio of $I_{8510} \equiv L_{8510}/L_{9170}$ and the metallicity for stellar populations older than 1 Gyr was found (Eq. (4) of Kong et al. 2000),

$$Z = (0.83 - 0.84 \times I_{8510})^2. \qquad (7)$$

4.2. Results

Using Eq. (7), we can calculate the metallicities of these old star clusters. We obtained $I_{8510} \equiv L_{8510}/L_{9170}$ using the photometric magnitudes in BATC13 and BATC14 bands (see Table 3). Then, the metallicities can be obtained using Eq. (7). The results are listed in Table 4 ([Fe/H] = $\log Z - \log Z_\odot$). The uncertainties for the metallicities are just the formal errors, since Kong et al. (2000) did not discuss any errors and uncertainties when they derived Eq. (7). The formal errors are obtained in the following way. Random values are selected for the observed data such that they obey a normal distribution, with sigma determined by the known errors in each sampled bin. We then obtain the best-fit metallicity. This procedure was repeated 300 times, giving us 300 separate determinations of the best-fit metallicity. The statistical standard deviation of metallicity from this procedure is adopted as the final error for the metallicity. In Table 4, we also present the ages for the sample clusters from Ma et al. (2001, 2002a,b,c). Table 5 lists some sample cluster metallicities from other authors (Cohen et al. 1984; Christian & Schommer 1988; Brodie & Huchra 1991; Sarajedini et al. 1998). Using two

Table 4. Metallicities of 31 old star clusters in M 33.

Cluster	$B - V$	$V - I$	[Fe/H]	log age (yr)
U 49	0.68	1.029	-1.75 ± 0.036	9.60
R 12	1.03	1.154	-1.46 ± 0.036	10.00
R 14	0.98	1.311	-0.63 ± 0.036	9.11
M 9	0.69	1.016	-1.17 ± 0.108	9.63
U 77	0.67	0.994	-0.76 ± 0.048	9.20
H 38	0.73	1.070	-0.84 ± 0.036	9.70
C 20	0.77	1.045	-1.30 ± 0.072	9.95
C 38	0.73	0.883	-2.12 ± 0.108	9.28
H 10	0.96	1.243	-0.74 ± 0.036	9.90
U 137	0.83	1.099	-0.20 ± 0.072	10.27
CBF 11	...	...	-1.30 ± 0.240	10.30
CBF 20	...	...	-0.44 ± 0.240	9.54
CBF 22	0.513	...	-1.03 ± 0.481	9.26
CBF 28	0.794	...	-1.94 ± 0.240	9.80
CBF 49	0.824	...	-1.69 ± 0.481	9.34
CBF 59	...	...	-0.14 ± 0.120	9.11
CBF 69	...	1.061	-1.25 ± 0.120	9.76
CBF 74	...	1.061	-0.12 ± 0.120	9.32
CBF 77	...	0.438	-0.62 ± 0.240	9.01
CBF 87	...	1.151	-0.97 ± 0.120	10.06
CBF 97	...	1.015	-0.24 ± 0.120	10.28
CBF 112	...	0.846	-2.98 ± 0.240	9.21
CBF 118	...	0.983	0.13 ± 0.120	9.16
CBF 119	...	0.940	0.17 ± 0.120	9.16
CBF 130	...	0.667	-1.63 ± 0.240	9.06
CBF 131	...	0.898	-1.19 ± 0.240	9.30
CBF 161	...	...	0.32 ± 0.120	10.28
M 5	0.73	1.32	0.06 ± 0.120	10.24
M 12	0.66	1.11	-0.54 ± 0.120	9.63
M 33	0.71	1.00	-1.51 ± 0.120	9.21
M 51	0.64	0.65	-1.41 ± 0.120	9.01

reddening-independent techniques, Cohen et al. (1984) obtained abundance estimates for the four GCs, M 9, U 49, H 38, and C 20. Comparing the results for these four clusters, we find that the only very discrepant result is for M 9, which we derive to be moderately metal rich, while Cohen et al. (1984) estimated it to be very metal poor. However, the results of Christian & Schommer (1988) and Sarajedini et al. (1998) for M 9 are intermediate between Cohen et al. (1984) and this study. Christian & Schommer (1988) and Brodie & Huchra (1991) estimated the metallicities for the 10 GCs using integrated spectra. The mean metallicity difference (the values of this paper minus the values of Christian & Schommer 1988; Brodie & Huchra 1991) is $< \Delta$[Fe/H] $> = 0.153 \pm 0.192$. Sarajedini et al. (1998) estimated the metallicities for these 10 GCs based on the shape and color of the red giant branch. Our results are consistent with Sarajedini et al. (1998) except for C38, which we find is very metal poor, but Sarajedini et al. (1998) find it to be the most metal rich. The mean metallicity difference (the values of this paper minus the values of Sarajedini et al. 1998) is $< \Delta$[Fe/H] $> = 0.148 \pm 0.216$. Sarajedini et al. (2000) estimated the cluster metallicities using the integrated $B - V$ colors from Christian & Schommer (1988) and the equations of Couture et al. (1990), and presented that the metallicity of R12 is very metal rich. Except for this cluster, our results are also consistent with the ones obtained using $B - V$ colors,

and the mean difference ($< $[Fe/H]$_{\text{This paper}} - $[Fe/H]$_{B-V} >$) is 0.056 ± 0.273.

5. Some properties of old star clusters

The following statistical relations are based on our data and are thus model-dependent.

5.1. Metallicity as a function of deprojected distance

Vílchez et al. (1988) studied the abundance gradient in M 33 on the data of emission lines in selected HII regions. The O/H gradient is steep in the inner regions, but much flatter in the outer regions, and N/O is constant over most of the visible disk, but lower in the outer HII region. We can investigate the radial abundance behavior of the old clusters in M 33. Using the data of both the red and blue portions of the instability trip of two halo globular clusters (M 9 and U 77) and the RR Lyrae luminosity relation, Sarajedini et al. (2000) estimated M 33 to be at a distance of $(m - M)_0 = 24.84 \pm 0.16$, which is adopted in this paper. We also adopted the inclination and position angles to be 56° and 23° of M 33, respectively (Regan & Vogel 1994). When the line of intersection (i.e. the major axis of the image) between the galactic plane and tangent plane is taken as the polar axis, it is easily proved that

$$r = \rho \sqrt{1 + \tan^2 \gamma \sin^2 \theta} \qquad (8)$$

and

$$\tan \phi = \frac{\tan \theta}{\cos \gamma}, \qquad (9)$$

where r and ϕ are the polar co-ordinates in the galactic plane, and ρ and θ are the corresponding co-ordinates in the tangent plane, and γ is the inclination angle of the galactic disk. Using formula (8), we can obtained the distances of our sample clusters from the center of M 33. Figure 2 displays the variation of metal abundance with deprojected radial position in units of kpc for 23 globular cluster candidates in M 33. This figure presents no relationship between the metal abundance of a cluster and its distance from the galactic center. This conclusion is consistent with that in Sarajedini et al. (2000) for the 9 GCs in this galaxy. Figure 3 plots the variation of metal abundance with deprojected radial position for all old clusters in this study.

5.2. Age as a function of deprojected distance

In Fig. 4, we plot the relation between age and galactocentric distance for 23 "true" GCs of M 33. Here we note that no relationship exists. This conclusion is consistent with Sarajedini & King (1989) and Chaboyer et al. (1996) for the GCs in the Galaxy. Figure 5 shows this relation for all 31 old clusters in this study, and no relationship can be found, too.

6. Summary and discussion

In this paper, based on the results of multicolor spectrophotometry in Ma et al. (2001, 2002a,b,c) and on the formula of

Table 5. Comparison of metallicity estimates with previous measurements.

Cluster	[Fe/H][a]	[Fe/H][b]$_{CPS}$	[Fe/H][c]$_{CS}$	[Fe/H][d]$_{BH}$	[Fe/H][e]$_{S}$
U 49	−1.75 ± 0.036	−1.4	−0.8 ± 0.3	−1.70 ± 0.53	−1.64 ± 0.20
R 12	−1.46 ± 0.036	...	−1.2 ± 0.3	...	−1.19 ± 0.24
R 14	−0.63 ± 0.036	...	−1.5 ± 0.3	...	−1.00 ± 0.50
M 9	−1.17 ± 0.108	−2.2	−1.7 ± 0.3	...	−1.64 ± 0.28
U 77	−0.76 ± 0.048	...	...	−1.77 ± 0.77	−1.56 ± 0.30
H 38	−0.84 ± 0.036	−1.0	−1.5 ± 0.3	...	−1.10 ± 0.10
C 20	−1.30 ± 0.072	−1.1	−2.2 ± 0.3	−1.25 ± 0.79	−1.25 ± 0.22
C 38	−2.12 ± 0.108	...	−1.2 ± 0.3	...	−0.65 ± 0.16
H 10	−0.74 ± 0.036	...	...	−0.91 ± 0.90	−1.44 ± 0.26
U 137	−0.20 ± 0.072	...	...	−0.12 ± 0.38	−0.98 ± 0.16

[a] This paper.
[b] Cohen et al. (1984).
[c] Christian & Schommer (1988).
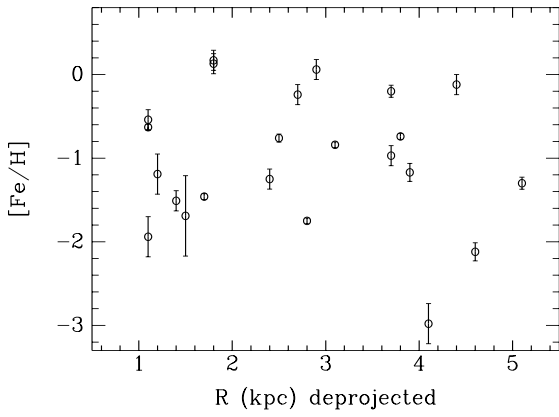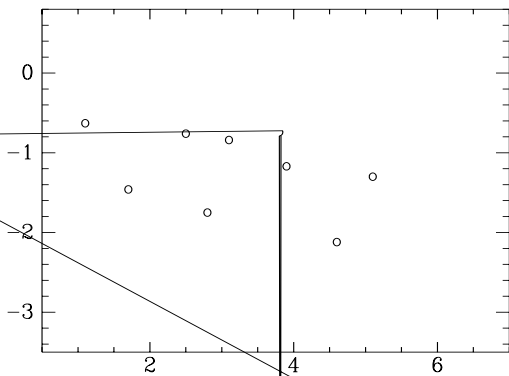[d] Brodie & Huchra (1991).
[e] Sarajedini et al. (1998).

Fig. 2. Deprojected radial variation of metal abundance for 23 "true" GCs of M 33.

As we know, the old stellar populations and the nuclei of spiral galaxies are dominated by G, K and M stars and therefore emit bulk of their light in the near infrared region of the spectrum. The CaT feature has been the subject of several analyses. Different authors emphasized its different utilizations, such as a luminosity indicator, and a possible discriminator between the light contribution due